

Project Title: **Enhanced Power Stability for Proton Conducting Solid Oxides Fuel Cells**

Type of Report: Final Report

Reporting Period Start Date: September 30, 2002

Reporting Period End Date: September 29, 2005

Principle Authors: Boris Merinov, William A. Goddard III, Sossina Haile, Adri van Duin, Peter Babilo, and Sang Soo Han

Date Report was Issued: December 29, 2005

DOE Award Number: DE-FC26-02NT41631

Name and Address of Submitting Organization: California Institute of Technology, mail code 139-74, 1200 E. California Blvd., Pasadena, CA 91125

DISCLAIMER

This report was prepared as an account of work sponsored by an agency of the United States Government. Neither the United States Government nor any agency thereof, nor any of their employees, makes any warranty, express or implied, or assumes any legal liability or responsibility for the accuracy, completeness, or usefulness of any information, apparatus, product, or process disclosed, or represents that its use would not infringe privately owned rights. Reference herein to any specific commercial product, process, or service by trade name, trademark, manufacturer, or otherwise does not necessarily constitute or imply its endorsement, recommendation, or favoring by the United States Government or any agency thereof. The views and opinions of authors expressed herein do not necessarily state or reflect those of the United States Government or agency thereof.

ABSTRACT

In order to provide the basis for a rational approach to improving the performance of Y-doped BaZrO₃ electrolytes for proton conducting ceramic fuel cells, we carried out a series of coupled computational and experimental studies to arrive at a consensus view of the characteristics affecting the proton conductivity of these systems.

The computational part of the project developed a practical first principles approach to predicting the proton mobility as a function of temperature and doping for polycrystalline systems. This is a significant breakthrough representing the first time that first principles methods have been used to study diffusion across grain boundaries in such systems. The basis for this breakthrough was the development of the ReaxFF reactive force field that accurately describes the structure and energetics of Y-doped BaZrO₃ as the proton hops from site to site. The ReaxFF parameters are all derived from an extensive set of quantum mechanics calculations on various clusters, two dimensionally infinite slabs, and three dimensionally infinite periodic systems for combinations of metals, metal alloys, metal oxides, pure and Y-doped BaZrO₃, including chemical reaction pathways and proton transport pathways, structures.

The ReaxFF force field enables molecular dynamics simulations to be carried out quickly for systems with ~ 10,000 atoms rather than the ~ 100 or so practical for QM.

The first 2.5 years were spent on developing and validating the ReaxFF and we have only had an opportunity to apply these methods to only a few test cases. However these simulations lead to transport properties (diffusion coefficients and activation energy) for multi-granular systems in good agreement with current experimental results.

Now that we have validated the ReaxFF for diffusion across grain boundaries, we are in the position of being able to use computation to explore strategies to improve the diffusion of protons across grain boundaries, which both theory and experiment agree is the cause of the low conductivity of multi-granular systems. Our plan for a future project is to use the theory to optimize the additives and processing conditions and following this with experiment on the most promising systems.

The experimental part of this project focused on improving the synthetic techniques for controlling the grain size and making measurements on the properties of these systems as a function of doping of impurities and of process conditions. A significant attention was paid to screening potential cathode materials (transition metal perovskites) and anode electrocatalysts (metals) for reactivity with Y-doped BaZrO₃, fabrication compatibility, and chemical stability in fuel cell environment. A robust method for fabricating crack-free thin membranes, as well as methods for sealing anode and cathode chambers, have been successfully developed. Our Pt | BYZ | Pt fuel cell, with a 100 μm thick Y-doped BaZrO₃ electrolyte layer, demonstrates the peak power density and short circuit current density of 28 mW/cm² and 130mA/cm², respectively. These are the highest values of this type of fuel cell.

All of these provide the basis for a future project in which theory and computation are combined to develop modified ceramic electrolytes capable of both high proton conductivity and excellent mechanical and chemical stability.

TABLE OF CONTENTS

List of graphical materials	5
Introduction	7
Executive summary	7
Results and discussion	9
Theoretical.....	9
QM Methods	9
ReaxFF Development	9
Applications of ReaxFF to modeling of hydrogen diffusion in Y-doped BaZrO ₃ ...	15
Experimental.....	18
Synthesis of BaZr _{1-x} Y _x O _{3-δ}	18
Characterization of BaZr _{1-x} Y _x O _{3-δ}	19
Processing of Y-doped BaZrO ₃	20
Baseline fuel cell performance demonstration	23
Screening of potential cathode materials (transition metal perovskites)	25
Screening potential anode electrocatalysts (metals) for reactivity with BaZr _{1-x} Y _x O _{3-δ} , fabrication compatibility, and chemical stability in fuel cell environment	26
Conclusions	27
References	28
List of acronyms and abbreviations	30

LIST OF GRAPHICAL MATERIALS

Figure 1. QM- and ReaxFF results for the equations of states for various Zr-, Y-, and Ba-polymorphs.

Figure 2. QM- and ReaxFF results for the equations of state of various Y/Zr- alloy polymorphs.

Figure 3. QM- and ReaxFF results for the equations of state of various ZrO₂ polymorphs.

Figure 4. QM- and ReaxFF results for the equations of state of various Y₂O₃ polymorphs.

Figure 5. QM- and ReaxFF results for the equations of state of various BaO polymorphs.

Figure 6. Heats of formation (in kcal/mol) for Y-doped BaZrO₃-phases.

Figure 7. QM- and ReaxFF energies for for hydrogen migration barriers in Y-doped BaZrO₃.

Figure 8. QM- and ReaxFF results for Pt-H and Ni-H interaction.

Figure 9. ReaxFF MD simulation on Y-doped BaZrO₃ at T=1000 K, 700 ps. Hydrogen trajectories are shown by small white spheres.

Figure 10. Calculated hydrogen diffusion coefficients as a function of the inverse temperature.

Figure 11. Model of Y-doped BaZrO₃ with grain boundaries.

Figure 12. Trajectory of the hydrogen atoms in Y-doped BaZrO₃ with grain boundaries. ReaxFF MD simulation, T=1000 K, 100 ps.

Figure 13. Calculated and experimental proton diffusion coefficients in Y-doped BaZrO₃. Experimental data are taken from Ref. [16].

Figure 14. X-ray diffraction patterns of BYZ powders calcined at 1250°C for 10 hours.

Figure 15. Plot of the refinement of the BYZ lattice parameters.

Figure 16. Plot of the weight gain of BYZ in a CO₂ atmosphere.

Figure 17. Temperature dependence of the proton conductivity of BYZ for x=0.20, 0.30, 0.40.

Figure 18. Effect of transitional metal oxide additives sintering aids for BYZ.

Figure 19. Density of BYZ and BYZ-Zn₄ as a function of sintering temperature in air.

Figure 20. SEM surface micrograph of sintered BYZ-Zn₄ at 1300°C.

Figure 21. The bulk, total grain boundary, and specific grain boundary conductivity of BYZ-Zn4 as a function of temperature plotted in Arrhenius form.

Figure 22. Bulk Conductivity of BYZ (BYZ20) and Ba-deficient BYZ (BYZ20 Ba-def.) as a function of temperature.

Figure 23. SEM micrograph of BYZ20 after 4hrs (a) and 24hrs (b) of sintering at 1600C.

Figure 24. Measured EMF and temperature of BYZ15 versus time.

Figure 25. Voltage, power density versus current density in BYZ20 240 μ m electrolyte.

Figure 26. Impedance measurements in humidified oxygen and hydrogen symmetric cell at 600 °C and $p_{\text{H}_2\text{O}} = 0.03$ atm.

Figure 27. Bulk conductivity of three potential cathode materials (a) and total conductivity of the most promising cathode materials (b)

Figure 28. Micrograph of a cathode-supported thin-film cell, 20 μ m BYZ supported on $\text{BaZr}_{0.40}\text{Pr}_{0.40}\text{Gd}_{0.20}\text{O}_3$.

Figure 29. Cross section of 80 μ m electrolyte BYZ membrane sandwiched by porous BYZ layers (a) and Cross-section of 100 μ m electrolyte BYZ membrane on BYZ porous support (b).

INTRODUCTION

Fuel cells have the potential to solve many power and transportation needs of the 21st century. Solid Oxide Fuel Cells (SOFCs) are particularly attractive because of their high efficiencies (especially when integrated with thermal energy conversion devices that utilize the high quality waste heat available from SOFCs), their fuel flexibility, and their operability in the absence of precious metal catalysts. A key hurdle to the commercialization of SOFCs is their high cost, which, in part, is due to their high operating temperatures (800 – 1000°C) and associated restrictions on materials choices. Therefore, one of the most important challenges in the high-temperature fuel cell research is searching for alternatives to the standard SOFC electrolyte, yttria-stabilized zirconia (YSZ) that will enable reduced temperature operation (500 – 700°C). Such a promising alternative might be the family of proton conducting perovskites. Perovskite oxides are known as very important technological materials that show a number of physico-chemical properties, such as high-temperature superconductivity, ferroelectricity, piezoelectricity, as well as they can be just simple insulators. In many acceptor-doped perovskite-type oxides high protonic conductivity has been observed at elevated temperatures, when they are exposed to water vapor [1-6]. Along with reduced operating temperature in comparison to that of commercially produced SOFCs based on YSZ, doped perovskite oxides often exhibit very good chemical and mechanical stability, which make them attractive for potential applications in various electrochemical devices, in particular, in fuel cells, hydrogen sensors and hydrogen pumps. In addition to their reduced temperature operation, these perovskites, due to their proton transport properties, offer the possibility of application in a number of arenas including hydrogen sensors for molten metals, H₂/D₂ separators, and hydrogen pumps. Y-doped BaZrO₃ (BYZ) ceramics is one of the most promising proton conducting materials for SOFC applications. It has desirable properties such as high protonic conductivity and excellent chemical and mechanical stability. The current limitation for application of BYZ in a proton ceramic fuel cell (PCFC) is the extremely high grain boundary resistance that leads to the relatively poor total conductivity. To understand the conduction process (both bulk and grain boundary) at the molecular level, we are developing the multi-scale strategy based on accurate quantum mechanics (QM) calculations of the relevant materials which are then used to derive a first principles-based reactive force field (ReaxFF) to perform large-scale molecular dynamics (MD) simulations that enable the study of proton transport under realistic conditions. This approach allows close cooperation between theorists and experimentalists, in which experiments are used to validate the computational predictions as well as to formulate new problems and tasks for modeling.

EXECUTIVE SUMMARY

It is well recognized that lower operating temperature of a SOFC increases the range of materials that can be used to construct the device and significantly reduce the cost of fabrication and increase the reliability of SOFC stacks. The use of a proton-conducting BYZ electrolyte allows the cell operating temperature to be lowered to below 500°C, a temperature at which standard stainless steel can be employed for many components. To develop high power-density and low-cost SOFCs based on proton conducting electrolytes, work should focus on 1) development of modified electrolytes that exhibit both high proton conductivity and excellent chemical and mechanical stability; and 2) development of highly efficient electrocatalysts for the anodes and cathodes. The current strategy based on the traditional empirical approach to materials design, which relies on preparing,

modifying, and testing several compositions in series, is inadequate today's requirements. Computational methods in conjunction with experimental techniques is a promising alternative for attacking the problem.

The critical component of our approach that now makes such studies possible is that we have developed a ReaxFF reactive force field, which has ability to describe formation and dissociation of chemical bonds while carrying out large scale MD simulations. ReaxFF potentials are completely based on an extensive set of quantum mechanics calculations, which are very time-consuming. We spent 2.5 years on developing and validating the ReaxFF for a BYZ electrolyte and Pt and Ni anode materials. At present, the ReaxFF enables MD simulations to be carried out quickly for systems with $\sim 10,000$ atoms rather than the ~ 100 or so practical for QM. Although we have only had an opportunity to apply this method to only a few cases, however, the obtained results look very promising. The ReaxFF MD simulations lead to transport properties (diffusion coefficients and activation energy) for multi-granular BYZ systems in good agreement with current experimental results. The current limitation for application of BYZ in fuel cells is the extremely high grain boundary resistance that leads to the relatively poor total conductivity. Now that we have validated the ReaxFF for diffusion across grain boundaries, we are in the position of being able to use computation to explore strategies to improve the diffusion of protons across grain boundaries, as well as to study chemical processes at the anode/electrolyte interface.

The experimental part of this project focused on improving the synthetic techniques for controlling the grain size and making measurements on the properties of these systems as a function of doping of impurities and of process conditions. A significant attention was paid to screening potential cathode materials (transition metal perovskites) and anode electrocatalysts (metals) for reactivity with Y-doped BaZrO_3 , fabrication compatibility, and chemical stability in fuel cell environment. A robust method for fabricating crack-free thin membranes, as well as methods for sealing anode and cathode chambers, have been successfully developed.

All of these provide the basis for a future project in which theory and computation are combined to develop modified ceramic electrolytes capable of both high proton conductivity and excellent mechanical and chemical stability. Our plan for a future project is to use the theory to optimize the additives and processing conditions and following this with experiment on the most promising systems.

RESULTS AND DISCUSSION

THEORETICAL

QM Methods

QM calculations have been performed at $T = 0$ K using density functional theory (DFT) in the generalized gradient approximation (GGA) [7, 8] that yields excellent structural energetics for many oxides.

The Jaguar 5.0 program package [9] was employed for the *ab initio* cluster calculations. We used the hybrid B3LYP-functional. This functional combines exact Hartree–Fock exchange with the local exchange functional of Slater [10], and includes the Becke nonlocal gradient correction [11], the Vosko–Wilk–Nusair exchange functional [12], and the Lee–Yang–Parr local and non-local correlation functional [13].

The periodic QM calculations were carried out using the SeqQuest code [14], a Gaussian-based linear combination of atomic orbitals method. Pseudopotentials were employed to replace the core electrons. The basis sets were high-quality, optimized “double zeta plus polarization” contracted Gaussian functions.

Most of the QM results obtained for relevant condensed phases and cluster systems are then used to derive parameters for the ReaxFF, which is implemented in larger scale MD simulations. In addition, the QM calculations are directly used to gain insight into mechanisms of chemical reactions, local dynamics of proton migration, surface stabilities, etc.

ReaxFF Development

QM is not practical yet for studying the dynamical properties of larger molecules and solids. Therefore, in order to model characteristics of fuel cell materials it is useful to have force fields that accurately describe chemical reactions, diffusion and other dynamical properties. Unlike traditional force fields, the ReaxFF solely based on QM calculations is especially designed to describe chemical reactivity, dissociation and formation of chemical bonds, surfaces, defects, diffusion, etc. The basic structure of the ReaxFF is similar to that employed in many non-reactive force fields in which the system energy is divided up into various partial energy contributions:

$$E_{system} = E_{bond} + E_{over} + E_{under} + E_{lp} + E_{val} + E_{pen} + E_{tors} + E_{conj} + E_{vdWaals} + E_{Coulomb}$$

The fundamental difference is that the ReaxFF does not employ the rigid connectivity method to determine the location of chemical bonds but use the bond order method instead. These bond orders, directly calculated from interatomic distances and continuously updated, allow formation and dissociation of bonds during MD simulations.

To establish parameters for the ReaxFF, both cluster and periodic QM data are incorporated into the training set and the ReaxFF is trained to accurately reproduce these data. Figures 1-5 show examples of such work and compare the QM and ReaxFF results for relevant metals, alloys, and metal oxides. One can see that the ReaxFF well reproduces the corresponding QM results.

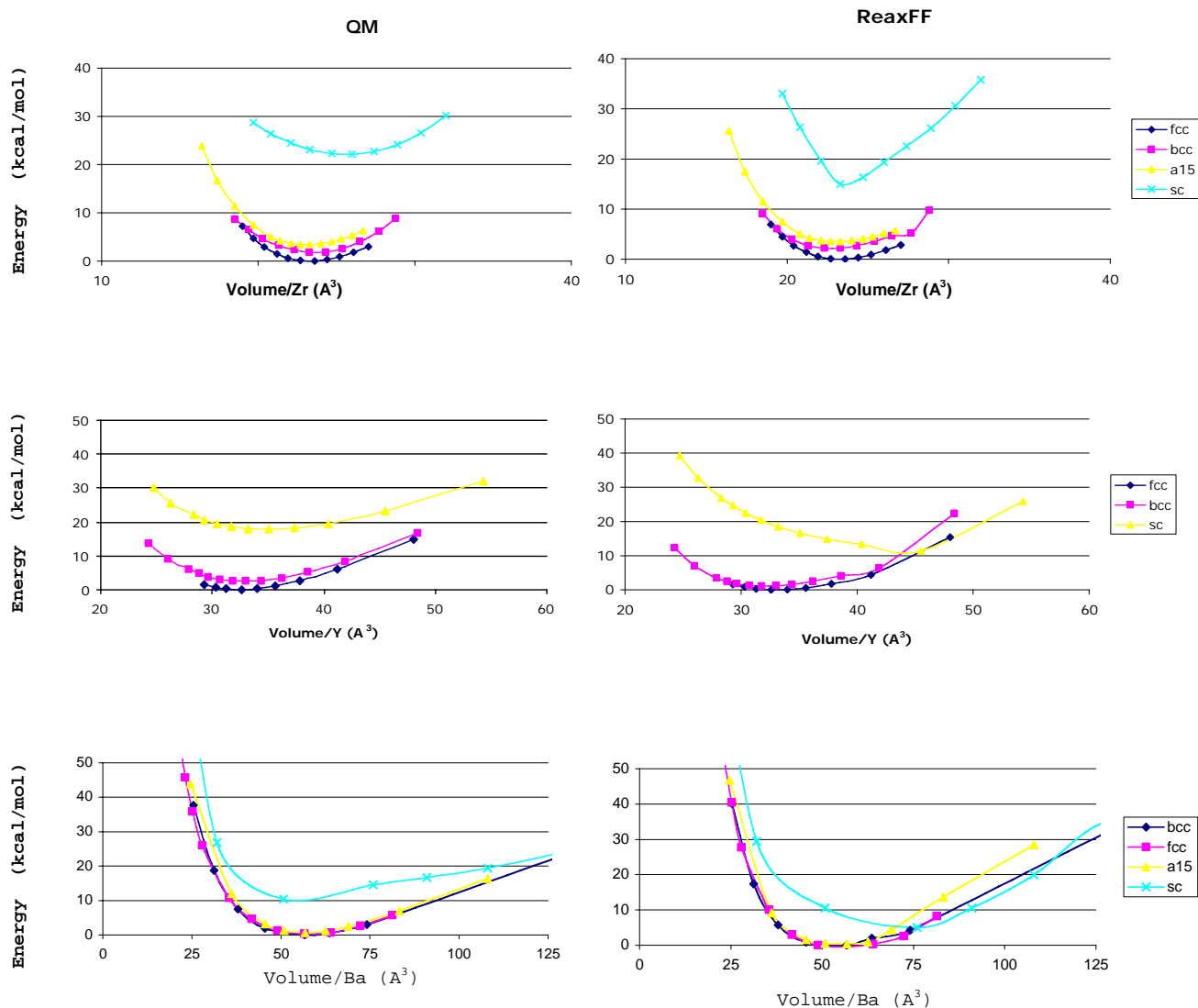


Figure 1. QM- and ReaxFF results for the equations of states for various Zr-, Y-, and Ba-polymorphs.

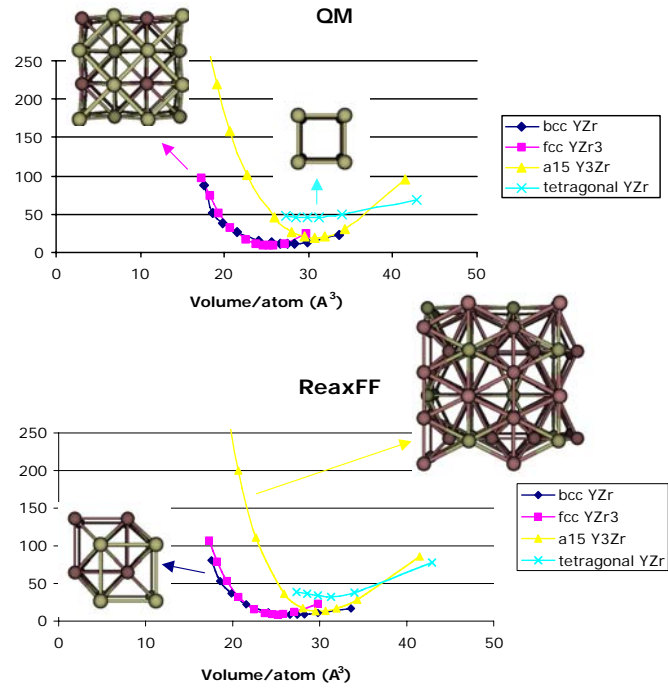


Figure 2. QM- and ReaxFF results for the equations of state of various Y/Zr- alloy polymorphs.

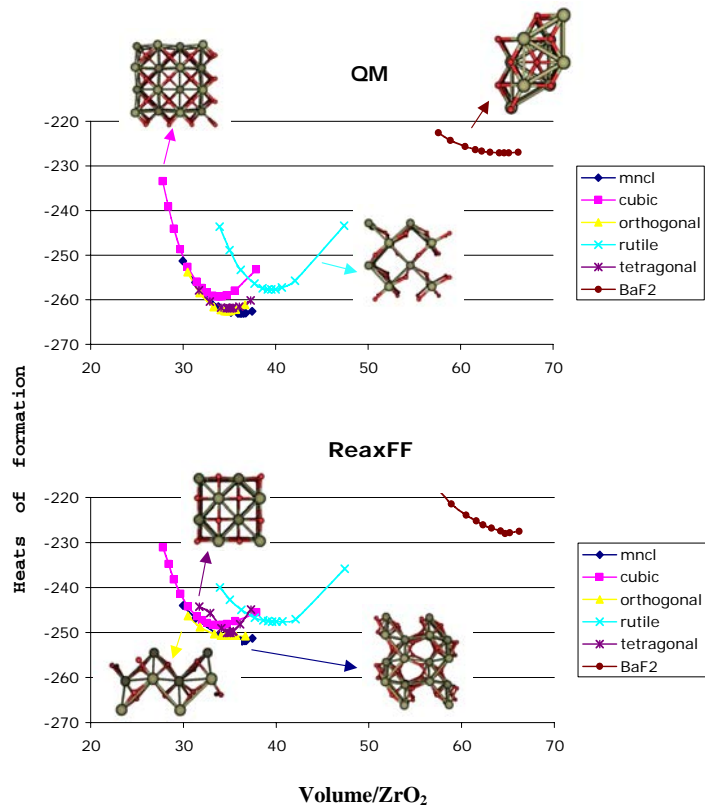


Figure 3. QM- and ReaxFF results for the equations of state of various ZrO_2 polymorphs.

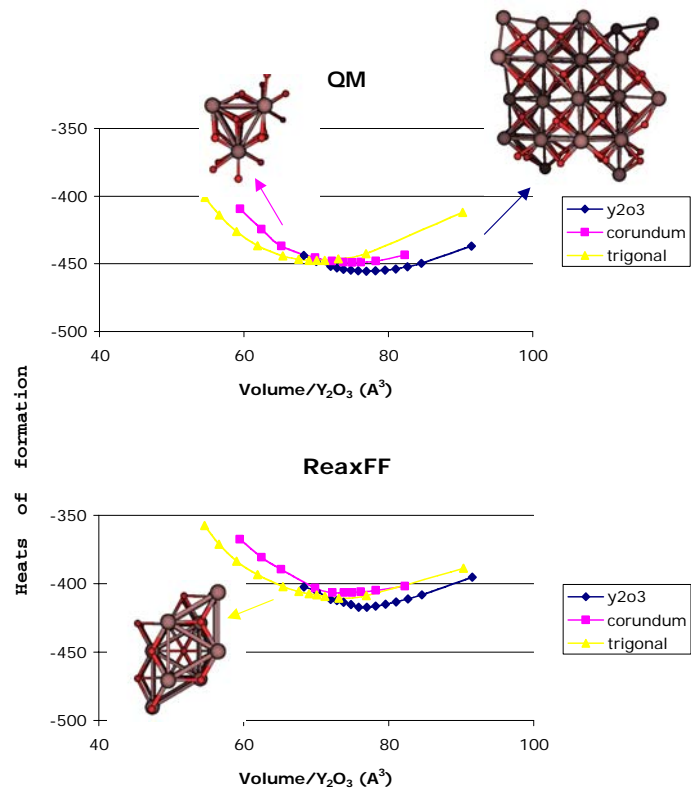


Figure 4. QM- and ReaxFF results for the equations of state of various Y_2O_3 polymorphs.

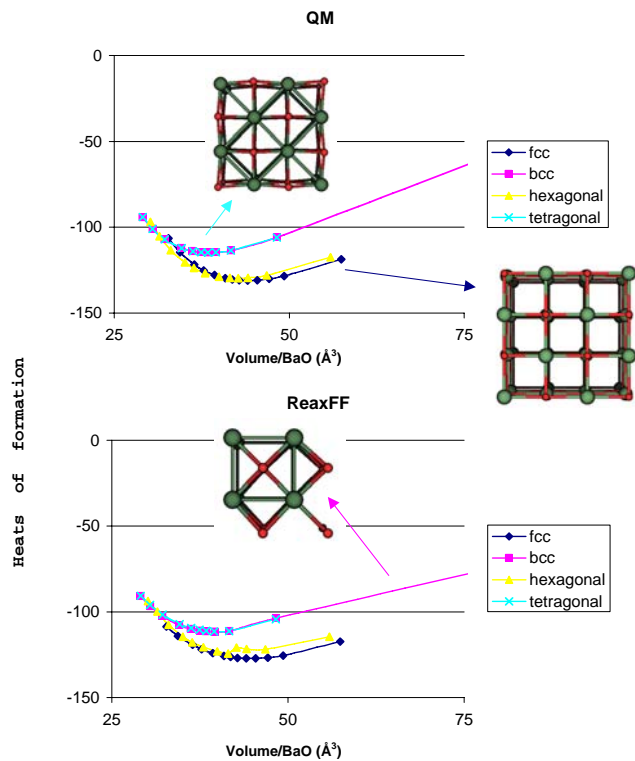


Figure 5. QM- and ReaxFF results for the equations of state of various BaO polymorphs.

In our work on developing ReaxFF potentials for the BYZ electrolyte we trained the ReaxFF to reproduce the QM relative energies and geometries for various structural configurations of BYZ in which the hydrogen atoms occupied various possible positions and we obtained good agreement between the QM and ReaxFF data (Figure 6).

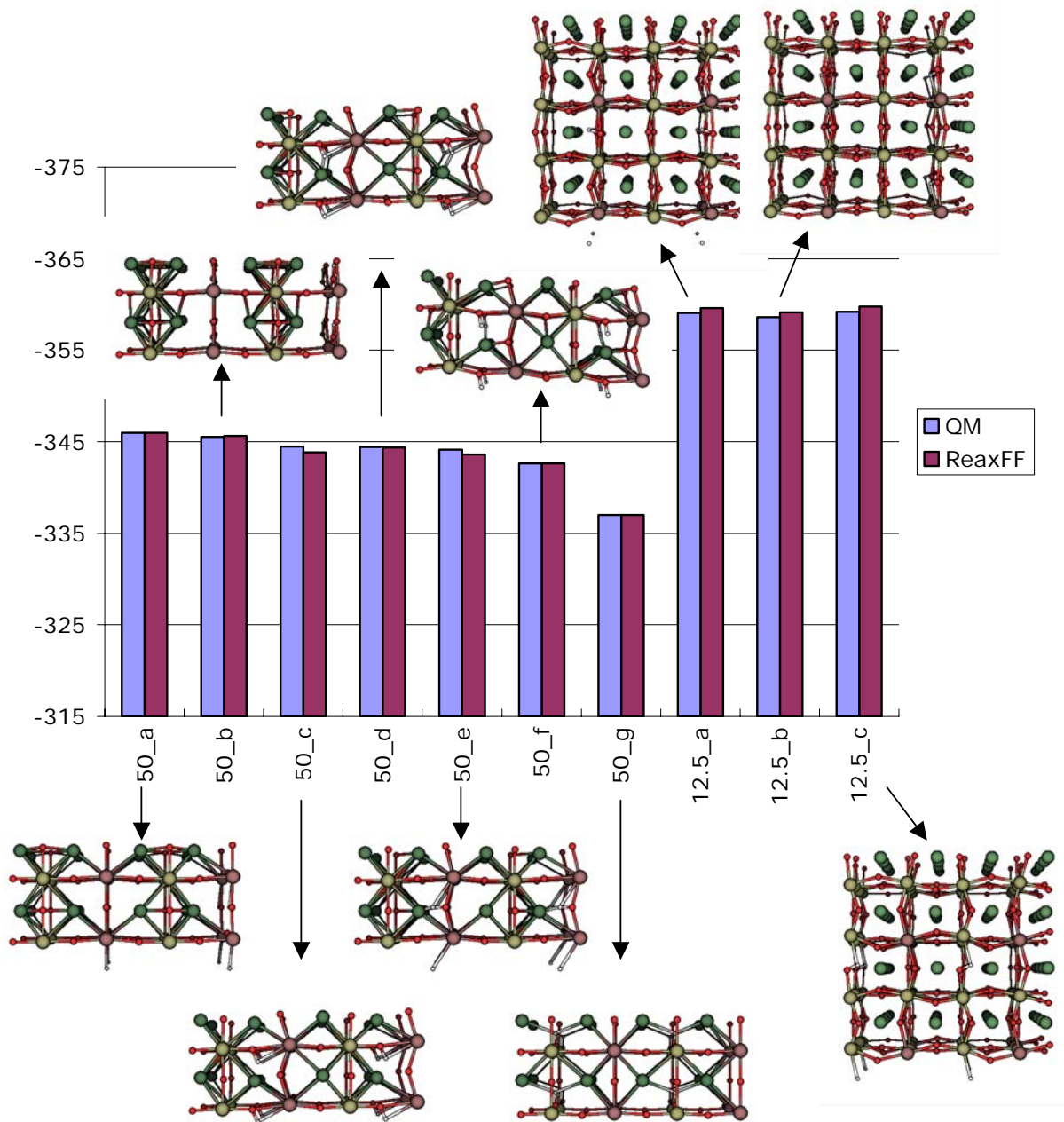


Figure 6. Heats of formation (in kcal/mol) for Y-doped BaZrO₃-phases.

The approach that we have employed to predict proton transport through the BYZ electrolyte is using QM to determine the barriers for H migration as a function of the donor-acceptor separation and then to combine probabilities based on these results with MD studies, allowing proton diffusion

when appropriate configurations are encountered. With ReaxFF we do not need to separate these processes since the reactions can occur during the dynamics. We validated the application of the ReaxFF to hydrogen transport through the BYZ electrolyte by fitting the ReaxFF parameters to QM-derived H-migration barriers. Figure 7 compares the QM and ReaxFF results for H-migration in BYZ as a function of oxygen-oxygen distances. It is clearly seen that the ReaxFF properly describes the distance-dependent hydrogen migration barriers and, therefore, the ReaxFF can be used in MD simulations to describe the proton transport in the BYZ electrolyte. Figure 7 also demonstrates that the hydrogen migration barriers are highly dependent on the distances between the donor and acceptor atoms: at short O-O distances the migration barriers virtually disappear.

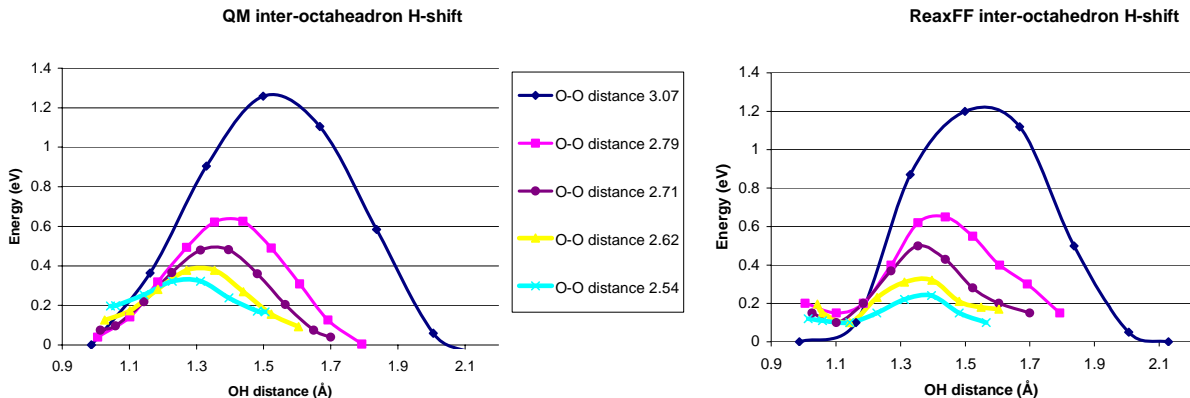


Figure 7. QM- and ReaxFF energies for for hydrogen migration barriers in Y-doped BaZrO₃.

From our QM calculations of the energy barriers for the hydrogen diffusion in BYZ, we also found possible proton pathways and concluded that both intra-Zr(Y)O₆-octahedron and inter-Zr(Y)O₆-octahedra proton transfers can occur in the BYZ electrolyte.

In fuel cells electrolytes are in contact with catalysts and electrodes forming membrane-electrode assemblies (MEAs). The electrolyte-electrodes interfaces are the primary source for power loss at small currents. Therefore, it is very important to develop computational tools for modeling interfaces. We started this work from the anode side, because our experimental study showed that majority of overpotential occurred at the anode rather than the cathode. The primary function of the anode in a PCFC is to facilitate the half cell reaction, $\frac{1}{2} \text{H}_2 \rightarrow \text{H}^+$ and e⁻ [assuming H₂ as the fuel]. If a hydrocarbon fuel is utilized, the anode must also catalyze the reformation of the fuel (which is mixed with H₂O) to produce CO₂ and H₂. Pt and Ni are particularly successful as the anode materials. We have carried out a series of QM calculations both on Pt and Ni and then used the obtained data for the development of the ReaxFF potentials. Figure 8 shows just one example of this work. From this Figure one can see that the ReaxFF very well reproduces the QM data and, therefore, can be used in further MD simulations of physico-chemical processes at the electrode/electrolyte interface.

To model BYZ/electrode interfaces and grain boundaries we also need a ReaxFF description of the oxide surfaces based on relevant QM data. We carried out QM calculations on various BaZrO₃ surfaces with different terminations using the SeqQuest code and then incorporated these data into the ReaxFF training set.

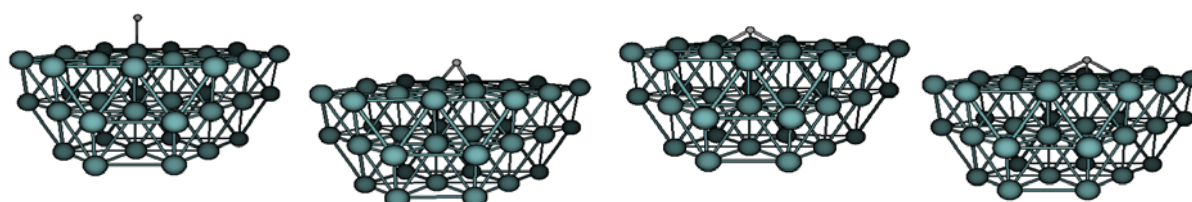
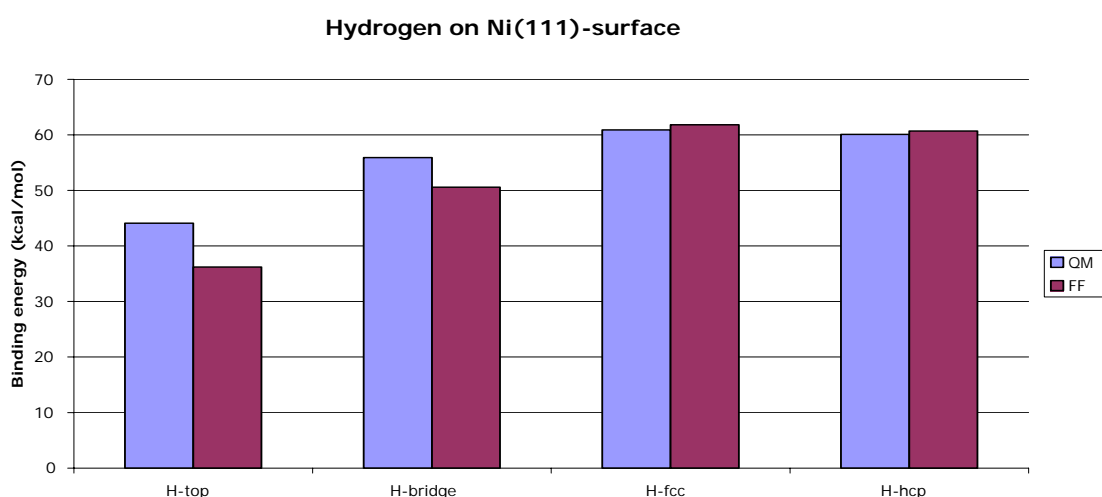
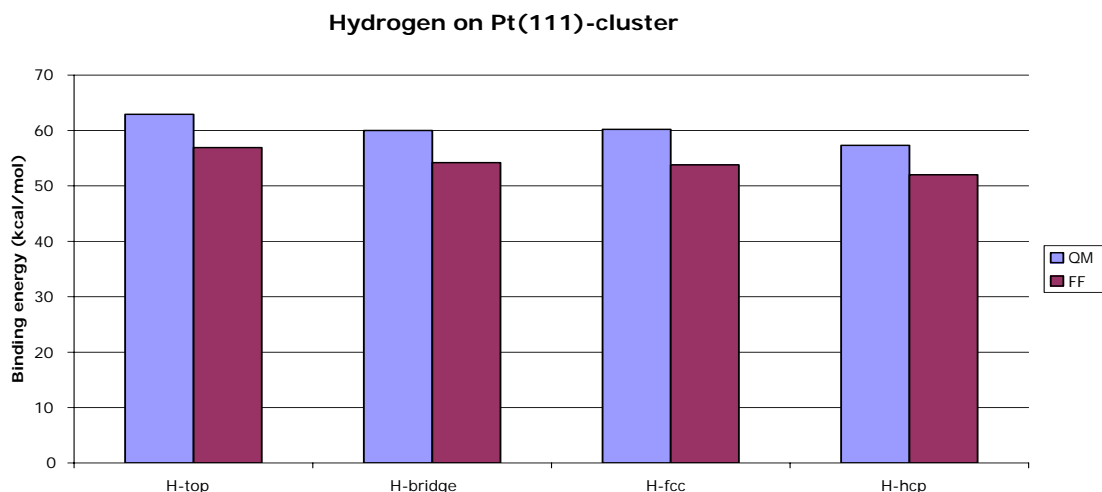


Figure 8. QM- and ReaxFF results for Pt-H and Ni-H interaction.

Applications of ReaxFF to modeling of hydrogen diffusion in Y-doped BaZrO₃

Based on the developed ReaxFF we have carried out MD simulations of the grain interior hydrogen diffusion in BYZ (328 atoms, including 8 hydrogen atoms) at different temperatures (750 K, 1000 K, 1250 K, and 1500 K). Figure 9 shows an example of such a modeling. Although hydrogen trajectories differ each from other and have their own particular features, all hydrogen atoms are highly mobile and the hydrogen transport is observed. The performed ReaxFF MD simulation allows us to calculate diffusion coefficients based on mean-square displacements and compare these data with experimental results. Figure 10 shows the calculated hydrogen diffusion coefficients as a function of the inverse temperature. It should be noted that the simulated results are in good agreement with the experimentally observed [15, 16]. This work is still in progress.

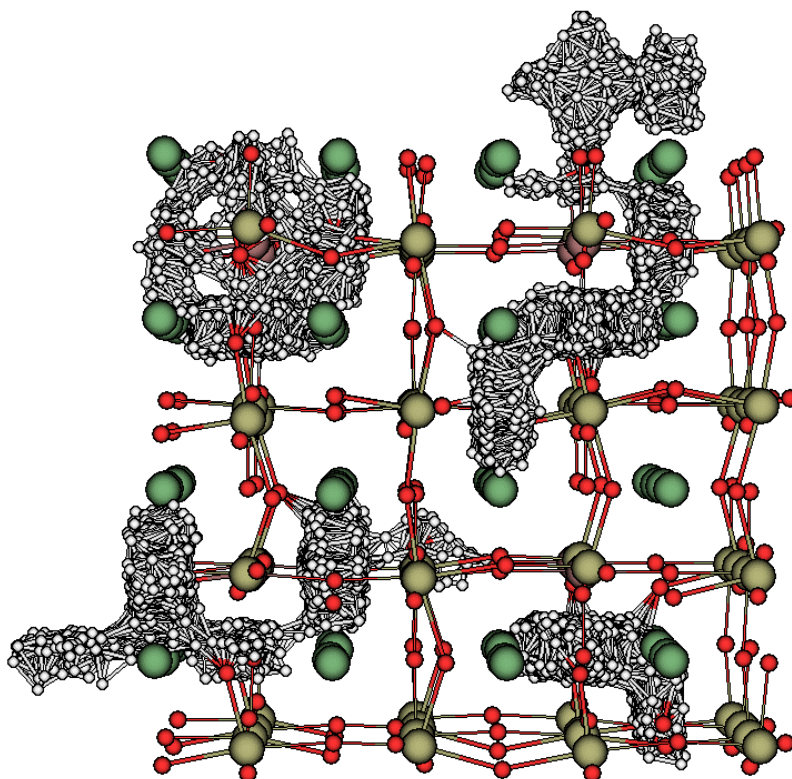


Figure 9. ReaxFF MD simulation on Y-doped BaZrO₃ at T=1000 K, 700 ps. Hydrogen trajectories are shown by small white spheres.

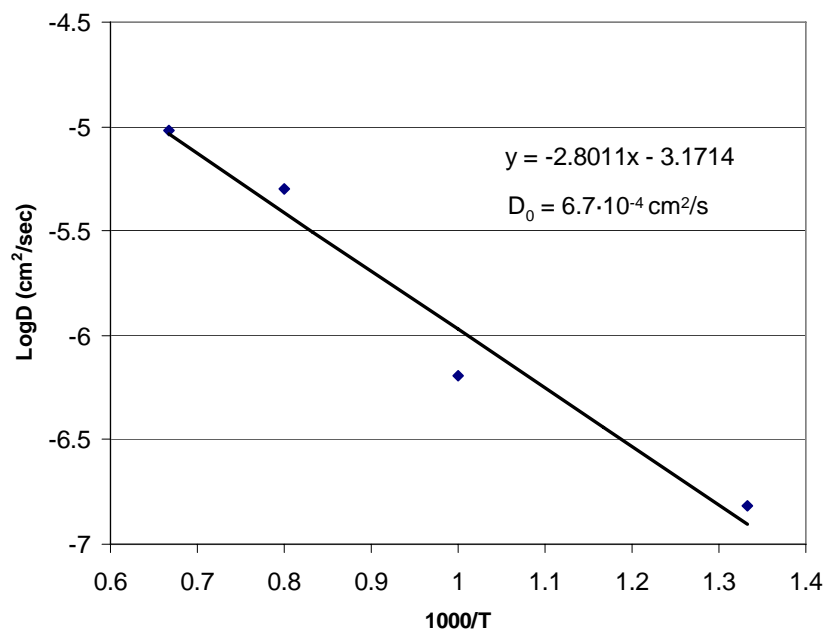


Figure 10. Calculated hydrogen diffusion coefficients as a function of the inverse temperature.

In proton-conducting ceramic systems, including BYZ, the total conductivity is very often limited by the grain-boundary conductivity. Experimentally, it is difficult to determine the structure of the grain boundaries at atomic level and, therefore, computational modeling might be a very useful tool to elicit useful information on the grain-boundary structure and to provide a deeper insight into grain, grain-boundary and total hydrogen diffusions in BYZ. Recently we have started ReaxFF MD simulations of the hydrogen diffusion on a BYZ model with grain boundaries (Figure 11). Preparing this model we took into account experimental data, which were obtained using electron microscopy [16].

Our initial ReaxFF MD simulations (872 atoms, including 16 hydrogen atoms, 100 ps) of the hydrogen diffusion at different temperatures (1000 K, 1250 K, 1500 K, 1750 K, and 2000 K) show that if the hydrogen comes into the grain boundary, it is stuck there for quite a long time within a limited volume (Figure 12). Actually, in these relatively short-time MD simulations (100 ps) we observed the proton transport across the grain boundary only at 1750 K and 2000 K and the hydrogen spent ~ 65 ps and ~ 25 ps in the grain boundary, respectively. We believe that our results are in agreement with the experimental data, which show that the grain boundaries decrease the total proton conductivity of BYZ [15].

Although the short-time MD simulations are not enough to make firm conclusions about the hydrogen transport in BYZ with grain boundaries, they nevertheless allowed us to calculate the preliminary hydrogen diffusion coefficients and compare these coefficients with the experimental ones (Figures 13). We found a good agreement between the simulated and experimentally observed diffusion coefficients. We also found that the activation

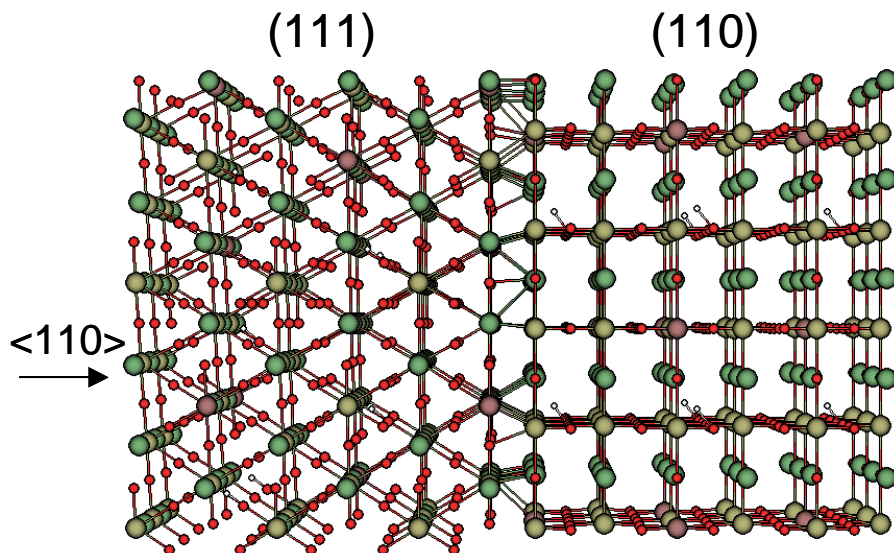


Figure 11. Model of Y-doped BaZrO₃ with grain boundaries.

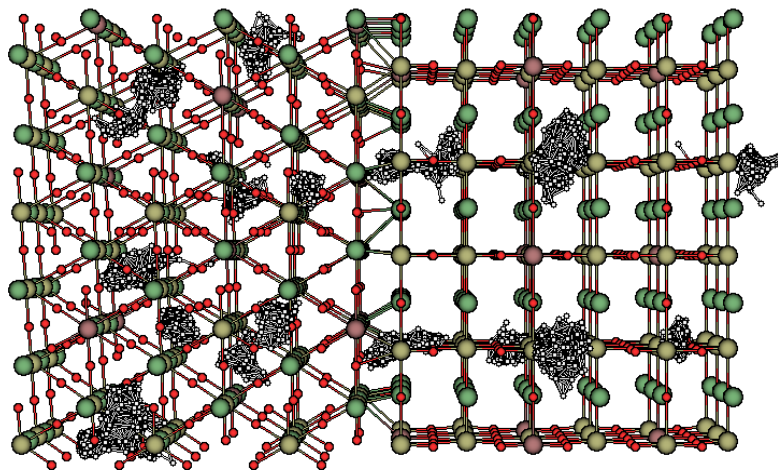


Figure 12. Trajectory of the hydrogen atoms in Y-doped BaZrO₃ with grain boundaries. ReaxFF MD simulation, T=1000 K, 100 ps.

energy is higher than the experimental one.

energy for the proton transport in BYZ calculated from our data, $E_a=0.45$ eV, is in very good agreement with that obtained in experiment, $E_a=0.44$ eV. Further work is in progress.

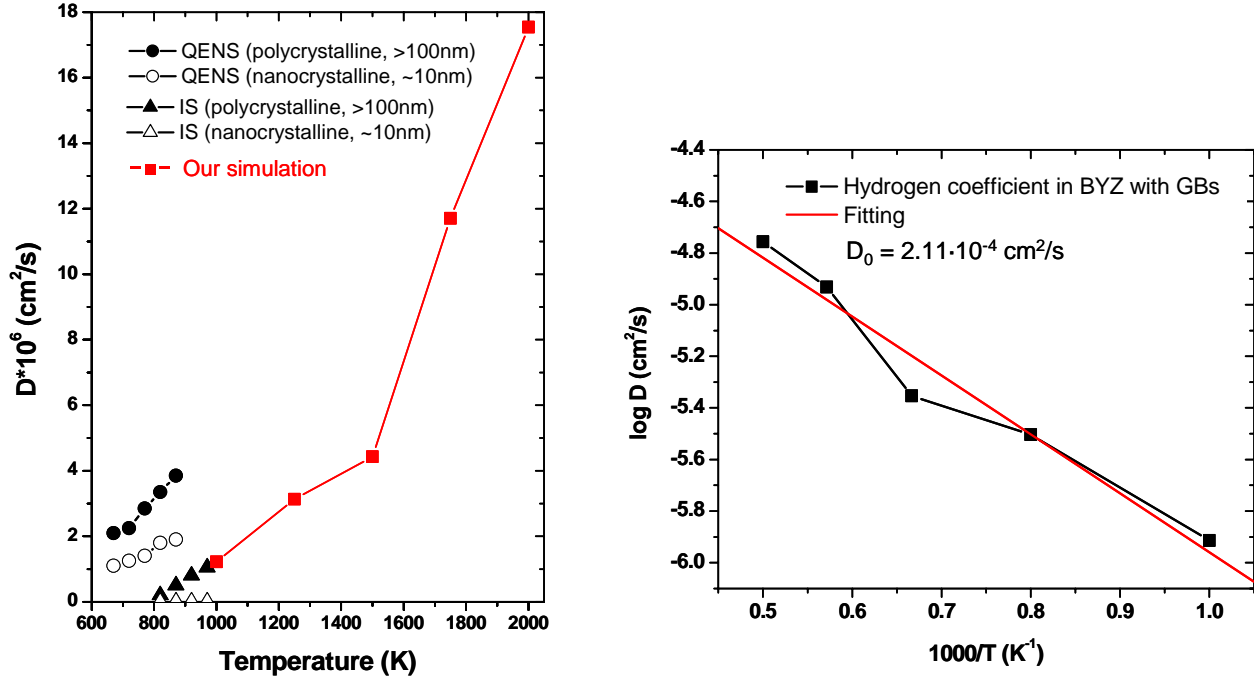


Figure 13. Calculated and experimental proton diffusion coefficients in Y-doped BaZrO₃. Experimental data are taken from Ref. [16].

EXPERIMENTAL

Synthesis of BaZr_{1-x}Y_xO_{3-δ}

BaZr_{1-x}Y_xO_{3-δ} with $x = 0.2, 0.3, 0.4, 0.5$ was synthesized by a modified Pechini route [17]. The precursors were Ba(NO₃)₂, Y(NO₃)₃·6H₂O and ZrO(NO₃)₂·xH₂O (x was determined by thermogravimetric analysis to be 1.96). EDTA and EG were used as polymerization/complexation agents at molar ratios of EDTA/ΣMetal = 2.0 and EDTA/EG=1/3. The powders derived were calcined at 1250°C for 10 hours.

XRD patterns of the samples were collected by a Philips X'pert Pro diffractometer using CuK α radiation. Figure 14 shows the XRD patterns of the powders calcined at 1250°C for 10 hours. The XRD patterns indicate that a single perovskite phase is formed in BaZr_{1-x}Y_xO_{3-δ} ($x = 0.2-0.5$). The peaks shift to the lower 2θ with increasing x , which could be explained by the ion size difference between Y³⁺ (0.892Å) and Zr⁴⁺ (0.72 Å). Therefore, the modified Pechini method can successfully be used for the synthesis of the proton conducting BaZr_{1-x}Y_xO_{3-δ} solid oxides with a wide range of the dopant concentration.

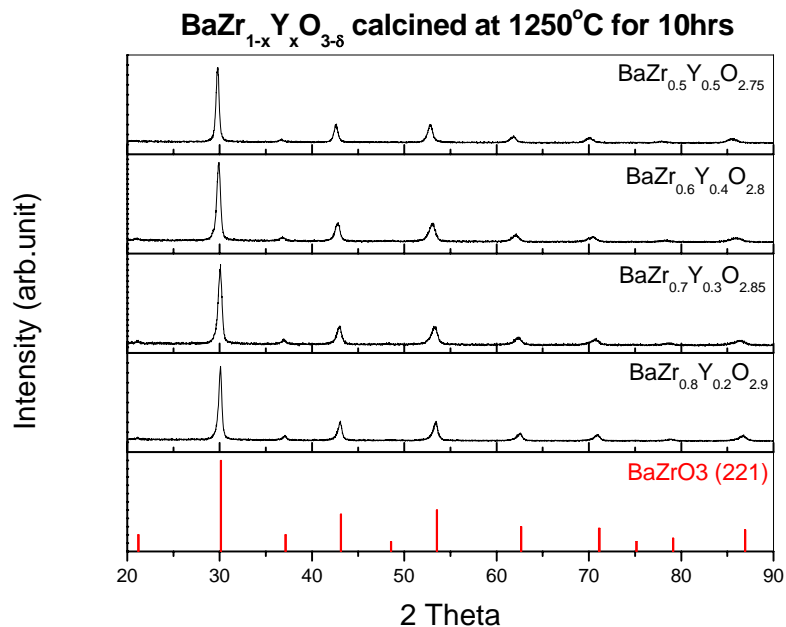


Figure 14. X-ray diffraction patterns of BYZ powders calcined at 1250°C for 10 hours.

Characterization of BaZr_{1-x}Y_xO_{3-δ}

The plot of the refinement of the BaZr_{1-x}Y_xO_{3-δ} lattice parameters is shown in Figure 15. The X'plus program was used to refine the cubic lattice parameters. It is clearly seen that the lattice parameters grow up with increasing x and at $x = 0.5$ (BaZr_{0.5}Y_{0.5}O_{2.75}) they reach the value of 4.2487(4) Å, cubic symmetry, space group $Pm-3m$.

A comparison of the thermal gravimetric behavior of BaZr_{1-x}Y_xO_{3-δ} and BaCeO₃ in the presence of CO₂ is presented in Figure 16. Consistent with earlier observations [18], gradual weight gain is apparent for the BaCeO₃ above 600°C signifying the formation of BaCO₃. In contrast, BaZr_{1-x}Y_xO_{3-δ} shows no significant weight gain. Thus, greater yttrium

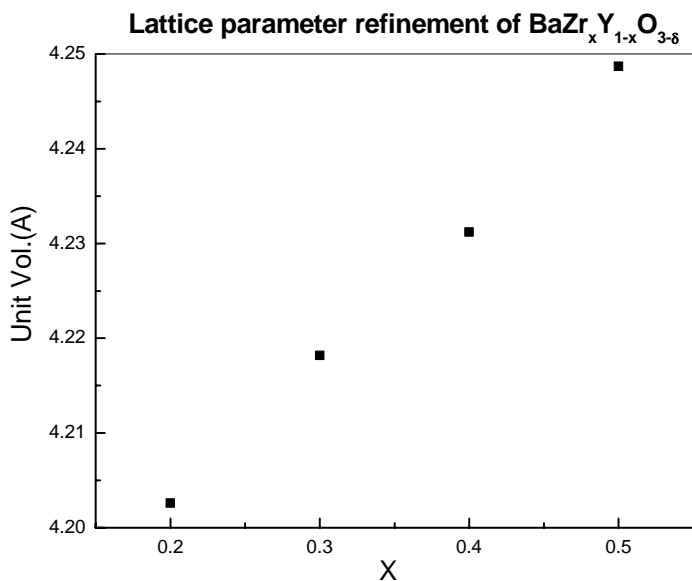


Figure 15. Plot of the refinement of the BYZ lattice parameters.

content does not impact the excellent stability of barium zirconate in carbon dioxide containing atmospheres.

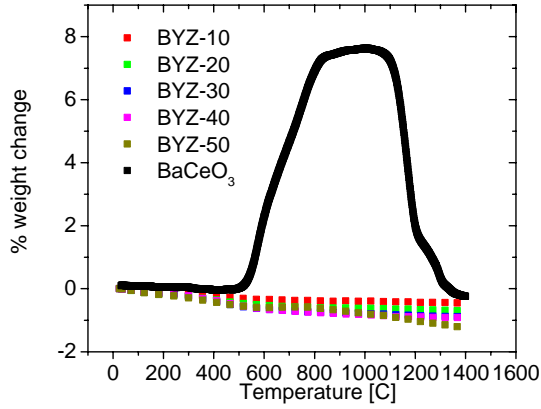


Figure 16. Plot of the weight gain of BYZ in a CO₂ atmosphere.

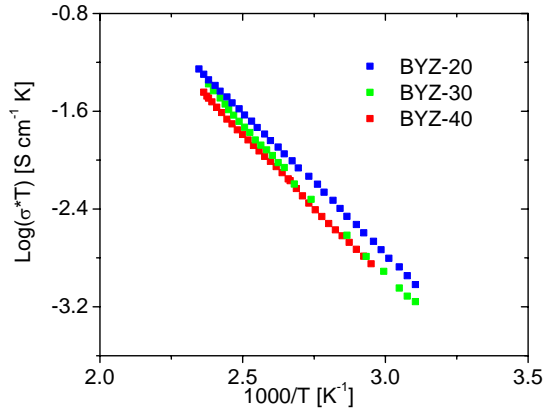


Figure 17. Temperature dependence of the proton conductivity of BYZ for $x=0.20, 0.30, 0.40$.

The transport property of $\text{BaZr}_{1-x}\text{Y}_x\text{O}_{3-\delta}$ for $x=0.20, 0.30, 0.40$ can be seen in Figure 17. The proton conductivity data were obtained from impedance spectroscopy over an extended temperature range. It is clear that the conductivity of $\text{BaZr}_{1-x}\text{Y}_x\text{O}_{3-\delta}$ decreases slightly with increasing yttrium dopant. It seems that the high concentration of the Y-dopant might lead to a trapping of the protons.

Processing of Y-doped BaZrO₃

As reported in literature, it is difficult to readily process BaZrO₃ to a high density (>93%). Usually extreme conditions, such as high temperature (1700-1800°C), long sintering times (24 h), and nanometer particle size are needed to prepare a fully densified pellet. Well-densified electrolyte is crucial for electrochemical cells because it allows for the separation of the reactants.

We have developed two unique processes in which we can reproducibly obtain 93-98% of theoretical density.

Process I, ZnO as a sintering aid

High temperature sintering to attain a dense sample is not practical for the development of thin-film supported electrolyte due to the fact that the cell components (electrolyte and support) need to be co-sintered. Decreasing the sintering temperature, as described below in Process I, will (i) allow for a wider range of materials to be used for the support, (ii) assist in better matching of thermal expansion of the components, and (iii) avoid the loss of barium, which has been previously reported to occur at high temperatures.

To accelerate the densification process at lower temperature, sintering aids were utilized. An initial screening of all transition elements in the series Sc to Zn, showed NiO, CuO and ZnO to be the most effective additives for enhancing barium zirconate densification, as shown in Figure 18. As evident from the data, Ni, Cu, and Zn enhanced densification from about 60% of theoretical for the

unmodified material to approximately 86-88% for modified BYZ, which later is improved to 95% with refined mixing techniques, Figure 19. Experimental details are provided in ref [19]. Other additives such as V, Cr and Fe, in contrast, substantially worsened densification behavior. Diffraction patterns after sintering for Ni, Cu, and Zn confirm a single perovskite phase. Upon closer examination under SEM (not shown here) equipped with EDS the Cu modified sample showed the presence of $Ba_2YCu_3O_x$ phase. Due to the presence of the second phase, Cu was eliminated as a modifier. The Ni modified BYZ pellets changed color to black after sintering, while the Zn modified changed to a light green. A color change from white to black usually suggests the presence of electronic conductivity. However, it should be noted that a minimal amount of transitional metal oxide was added, which is unlikely to significantly increase electronic conduction in the sample. Since Ni and Zn produce similar results and to be cautious of electronic conductivity, Zn was chosen as the best modifier.

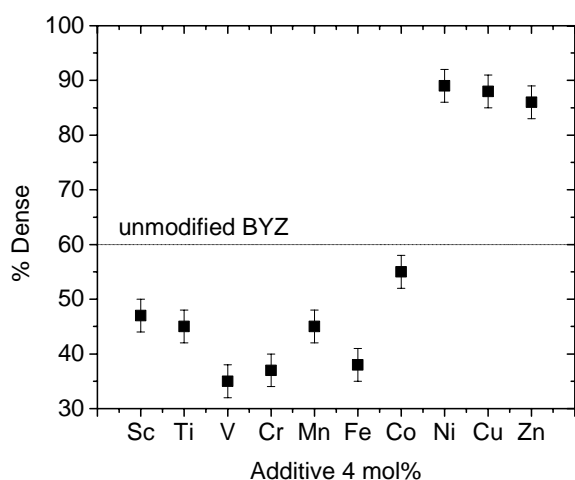


Figure 18. Effect of transitional metal oxide additives sintering aids for BYZ.

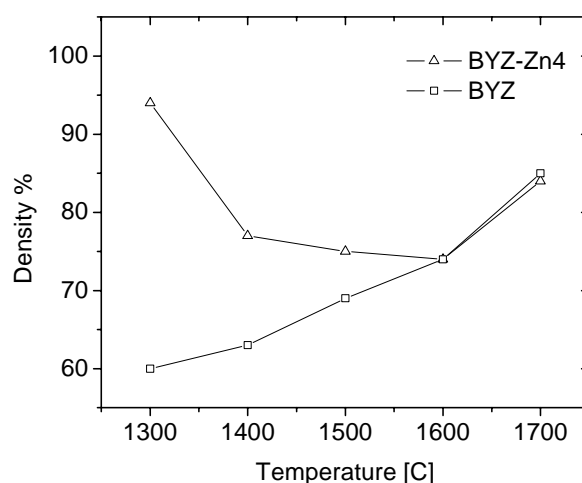


Figure 19. Density of BYZ and BYZ-Zn4 as a function of sintering temperature in air.

The difference in sintering behavior between unmodified and Zn-modified BYZ is particularly evident from a comparison of densities as a function of temperature, Figure 19. For BYZ-Zn4, the density reached 95% of theoretical value D_t ($D_t = 6.12 \text{ g/cm}^3$) at 1300°C compared to the maximum density of 88% for BYZ at 1700°C . Microstructure of the Zn-modified BYZ is highlighted in Figure 20. As can be seen, a dense surface was achieved with a homogenous grain size distribution and average grain size of $1 \mu\text{m}$.

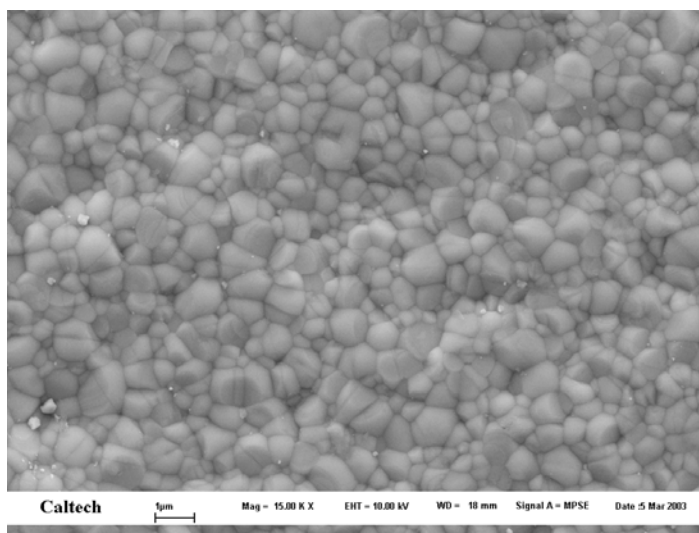


Figure 20. SEM surface micrograph of sintered BYZ-Zn4 at 1300°C .

The temperature dependence of the bulk conductivity σ_{gi} , grain boundary conductivity σ_{gb} , and specific grain boundary conductivity $\sigma_{sp,gb}$ are presented in Figure 21 for BYZ-Zn4. The bulk conductivity of BYZ agrees with the highest reported value [15], shown in the Figure 21. Bulk conductivity of the BYZ-Zn4 is slightly lower than that of unmodified BYZ. It is believed the lower bulk conductivity is a result of Ba loss per equation 1.



Process II, densification without the use of sintering aids

Both solid state and chemical synthesis were utilized to produce BYZ, and both methods proved suitable so long as the optimized procedure was followed. Optimized processing procedure of the BYZ system included (i) mechanical grinding of the loose powder to crystallite size of 50-100nm range prior to densification, (ii) Combination of the loose powder with a binder solution and subsequent sieving with 100 mesh sieve, (iii) Uniaxial pressing with 4.0 ton /cm² with a pre-calcination step to 700C, and (iv) Sintering at 1600C with excess BaO. This procedure allowed for reproducible densities of 93-97% without the use of sintering aids. In terms of electrical properties, the most critical step is the sintering with excess BaO. As shown in Figure 22, Ba loss during the sintering dramatically decreases the bulk conductivity of BYZ. We believe this is one significant factor that has led to the wide range of reported conductivities for BYZ. It is also clear that the measured BYZ20 has higher bulk conductivity compared to Bohn et al [3], which is expected due to the higher dopant concentration in this sample as opposed to Bohn’s BYZ10. Activation energy was measured as 0.46(±0.01)eV, comparable to 0.44eV measured by Bohn.

The development of a reproducible procedure for high density and high conductivity BYZ allowed for the observation of sintering time effects of the grain growth, Figure 23. Grain size can be modified from 0.40 μm after 4hrs sintering

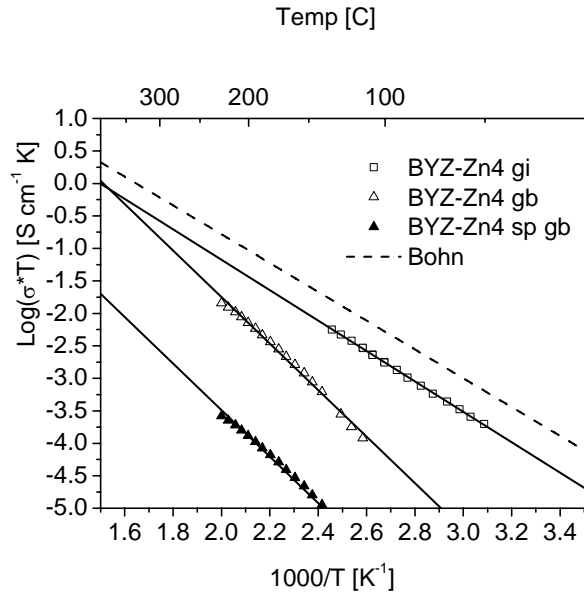


Figure 21. The bulk, total grain boundary, and specific grain boundary conductivity of BYZ-Zn4 as a function of temperature plotted in Arrhenius form.

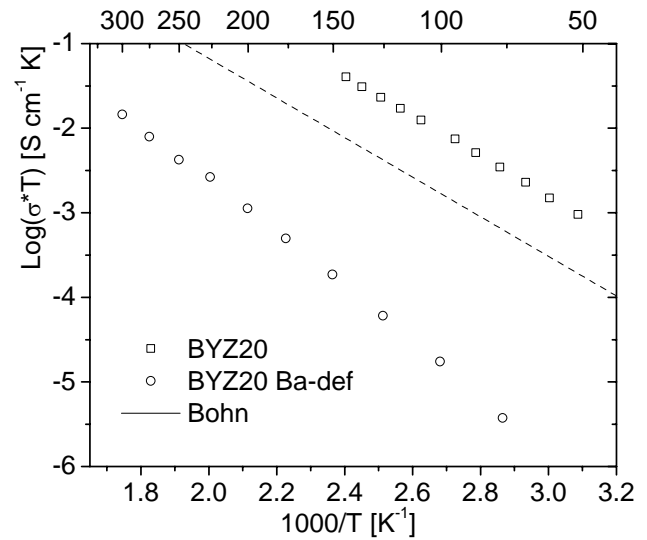


Figure 22. Bulk Conductivity of BYZ (BYZ20) and Ba-deficient BYZ (BYZ20 Ba-def.) as a function of temperature.

to 0.90 μm after 24 hrs sintering. Increased grain size will significantly increase the total conductivity of the material. As discussed previously, the grain boundary is the inhibiting contribution to the total conductivity. With less grain boundaries (24hr samples) it is expected to have a higher total conductivity (confirmed, but not shown here).

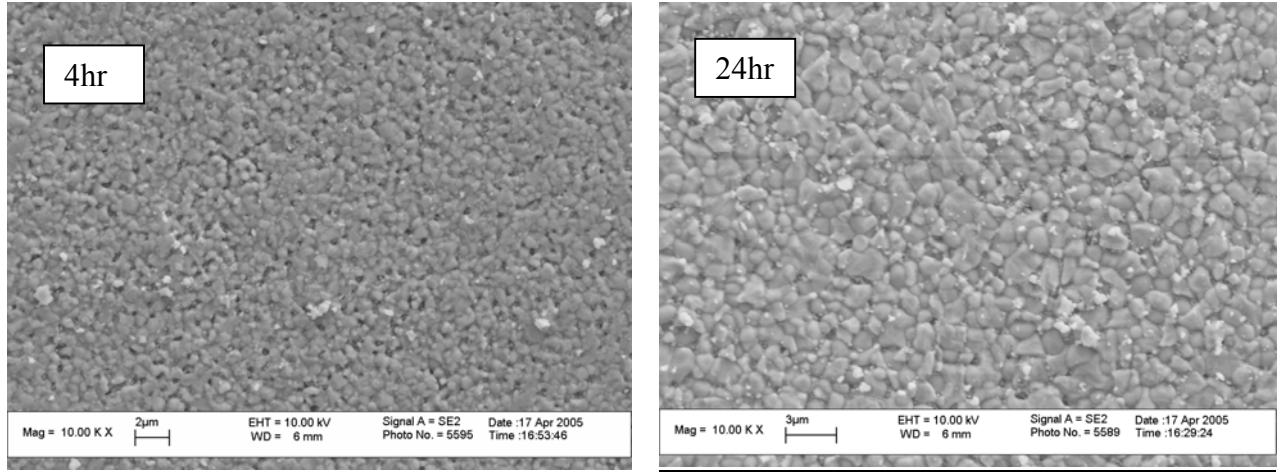


Figure 23. SEM micrograph of BYZ20 after 4hrs (a) and 24hrs (b) of sintering at 1600C.

Baseline fuel cell performance demonstration

The results of the EMF measurements are shown in Figure 24. Water saturated air was supplied to one chamber and water saturated hydrogen to the other. The data reveal the ion transport number of BYZ to be ~ 0.92 in the temperature range of interest, dropping slightly from 0.92 at 500°C to 0.88 at 700°C. By analogy to related materials the balance of the charge transport can be attributed to electron hole charge carriers. With increasing temperature, both the loss of water from the structure and the higher mobility of the holes lead to a slight decrease in ionic transport number. Overall, it is apparent that the ionic transport number of BYZ is sufficient for satisfactory implementation in a fuel cell.

Baseline fuel cell measurements were made with Pt painted on both sides of a thin membrane (240 μm). A maximum 25mW/cm² was achieved at 600C, Figure 25. While these values are not the highest reported for SOFCs,

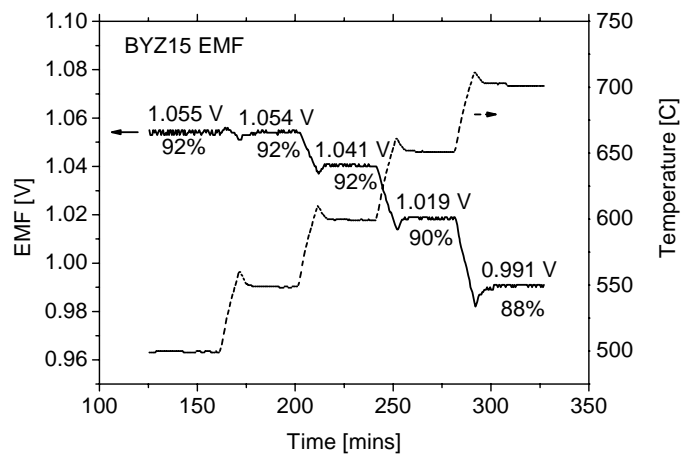


Figure 24. Measured EMF and temperature of BYZ15 versus time.

they are the highest values reported in the open literature for fuel cells based on doped barium zirconate.

Impedance measurements of symmetric cell in oxygen show a total resistance of $6.9 \text{ ohm}\cdot\text{cm}^2$ of which $4 \text{ ohm}\cdot\text{cm}^2$ is due to the electrolyte, Figure 26. This implies a cathode resistance of $1.45 \text{ ohm}\cdot\text{cm}^2$. Similarly an anode resistance of $5.5 \text{ ohm}\cdot\text{cm}^2$ is calculated. It is unusual for the anode to be the more resistive electrode, however it is the case in the BYZ system and it is speculated that under the reducing conditions the Pt reacts with the Zr. These tests suggest that the further optimization of the anode will lead to higher performance.

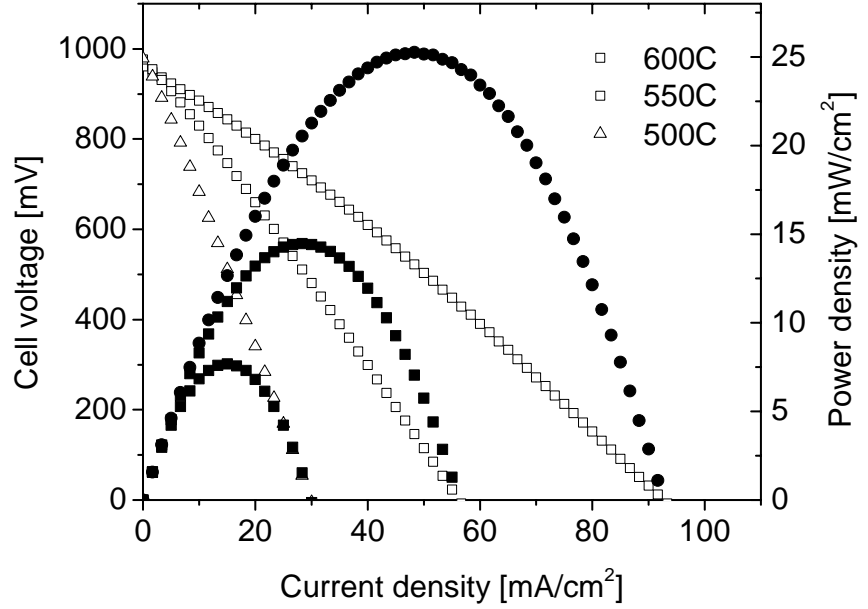


Figure 25. Voltage, power density versus current density in BYZ20 $240\mu\text{m}$ electrolyte.

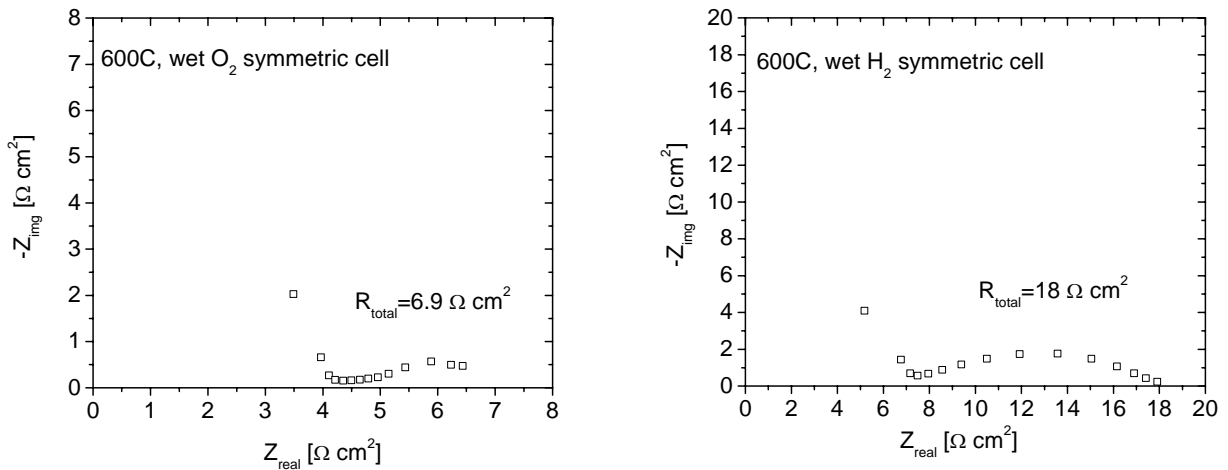


Figure 26. Impedance measurements in humidified oxygen and hydrogen symmetric cell at $600 \text{ }^\circ\text{C}$ and $p_{\text{H}_2\text{O}} = 0.03 \text{ atm}$.

Screening of potential cathode materials (transition metal perovskites)

Several potential cathode materials for the doped barium zirconate system were synthesized via the glycine nitrate combustion method. The appropriate metal-nitrates and a glycine to nitrate ratio of 1:2 was utilized. The following cathodes were synthesized: $\text{BaZr}_{0.40}\text{Pr}_{0.40}\text{Gd}_{0.20}\text{O}_3$, $\text{BaZr}_{0.70}\text{Pr}_{0.10}\text{Gd}_{0.20}\text{O}_3$, $\text{BaZr}_{0.80}\text{Co}_{0.20}\text{O}_3$, $\text{BaZr}_{0.60}\text{Y}_{0.20}\text{Co}_{0.20}\text{O}_3$, $\text{BaPr}_{0.85}\text{Y}_{0.15}\text{O}_3$, $\text{BaZr}_{0.55}\text{Y}_{0.15}\text{Pr}_{0.30}\text{O}_3$, and $\text{BaZr}_{0.70}\text{Y}_{0.15}\text{Pr}_{0.15}\text{O}_3$. All formed single phase perovskites as determined by X-ray power diffraction (data not shown). The Pr rich compound, $\text{BaPr}_{0.85}\text{Y}_{0.15}\text{O}_3$, however, proved to be unstable with time and at high temperature and was not considered further.

Potential cathodes were mixed with $\text{BaZr}_{0.85}\text{Y}_{0.15}\text{O}_3$ (BYZ) and calcined at 700°C (maximum fuel cell operating temperature) for 24 hours to observe the possibility of a reaction/interdiffusion. Under these conditions, $\text{BaZr}_{0.70}\text{Pr}_{0.10}\text{Gd}_{0.20}\text{O}_3$ and $\text{BaZr}_{0.80}\text{Co}_{0.20}\text{O}_3$ completely reacted with BYZ to yield a single, solid-solution perovskite phase and were not considered further. In contrast the remaining four materials did not react with BYZ and retained two perovskite phases, although the possibility of slight interdiffusion cannot be entirely ruled out. Samples with higher content zirconium (>0.70) proved to be most stable with time.

Bulk conductivity measurements as a function of temperature are shown in Figure 27a for the two of the most stable potential cathodes, and the total conductivity, Figure 27b, (bulk+grain boundary) is shown for the most promising material, $\text{BaZr}_{0.70}\text{Y}_{0.15}\text{Pr}_{0.15}\text{O}_3$. Again the benefits of an optimized densification procedure can be seen with the dramatically low conductivity of the Ba-deficient cathode.

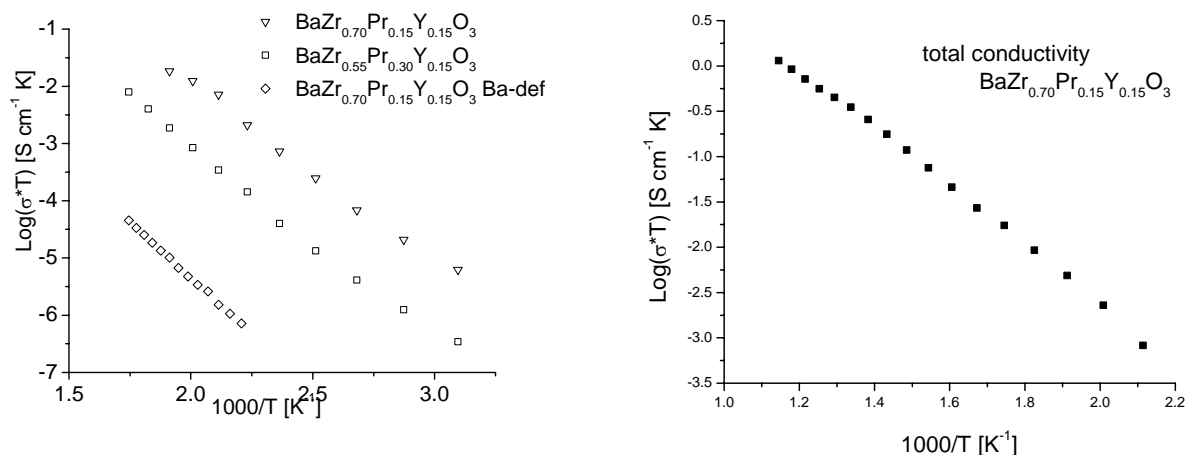


Figure 27. Bulk conductivity of three potential cathode materials (a) and total conductivity of the most promising cathode materials (b)

Development of cathode and electrolyte deposition methods

Two cathode deposition techniques, both based on colloidal methods, were pursued for the fabrication of electrolyte-supported (and ultimately anode-supported) fuel cells using potential

cathode materials, $\text{BaZr}_{0.40}\text{Pr}_{0.40}\text{Gd}_{0.20}\text{O}_3$, $\text{BaZr}_{0.60}\text{Y}_{0.20}\text{Co}_{0.20}\text{O}_3$, $\text{BaZr}_{0.55}\text{Y}_{0.15}\text{Pr}_{0.30}\text{O}_3$, and $\text{BaZr}_{0.70}\text{Y}_{0.15}\text{Pr}_{0.15}\text{O}_3$. In the first method, the colloidal solution was deposited onto BYZ by mechanical methods using a simple paintbrush. After calcination at 900°C for 2 hours, the cathode adhesion to the electrolyte was found to be poor and the cathode could be easily removed. Accordingly, the method was abandoned. In the second method, the colloidal solution was deposited by spraying. Better contact between the cathode and the electrolyte was achieved, particularly in the case of $\text{BaZr}_{0.60}\text{Y}_{0.20}\text{Co}_{0.20}\text{O}_3$, $\text{BaZr}_{0.55}\text{Y}_{0.15}\text{Pr}_{0.30}\text{O}_3$, and $\text{BaZr}_{0.70}\text{Y}_{0.15}\text{Pr}_{0.15}\text{O}_3$ justifying the greater effort involved in this method. In the case of $\text{BaZr}_{0.40}\text{Pr}_{0.40}\text{Gd}_{0.20}\text{O}_3$, although the contact was improved by spray deposition, the cathode eventually detached over time. It is believed that the introduction of a porous BYZ layer between the electrolyte and cathode will further improve the adhesion. Also was shown that Y and Zr containing cathodes adhere better to the BYZ electrolyte.

Fabrication of cathode-supported cells is also under development. Such structures would be implemented should the cathode overpotential be lower than that of the anode (which is the case at least for Pt cathodes). Our development of highly sinterable BYZ via the introduction of 4 mole % Zn (BYZ-Zn4) has made it possible to pursue cathode supported fuel cells. Fabrication methods to date have involved dual pressing, in which a thick cathode layer is uniaxially pressed and a thin electrolyte layer deposited atop this layer and the two layers pressed together (again, uniaxially). Sintering is carried out at $1300\text{--}1400^\circ\text{C}$, at which BYZ-Zn4 densification is greatest. Figure 28 shows a BYZ-Zn4 electrolyte on a $\text{BaZr}_{0.40}\text{Pr}_{0.40}\text{Gd}_{0.20}\text{O}_3$ cathode support. The electrolyte is approximately 40-50 micrometers thick, however it is not yet fully densified. Further optimization of the co-sintering temperature is needed to develop a thin dense electrolyte on a cathode supported MEA.

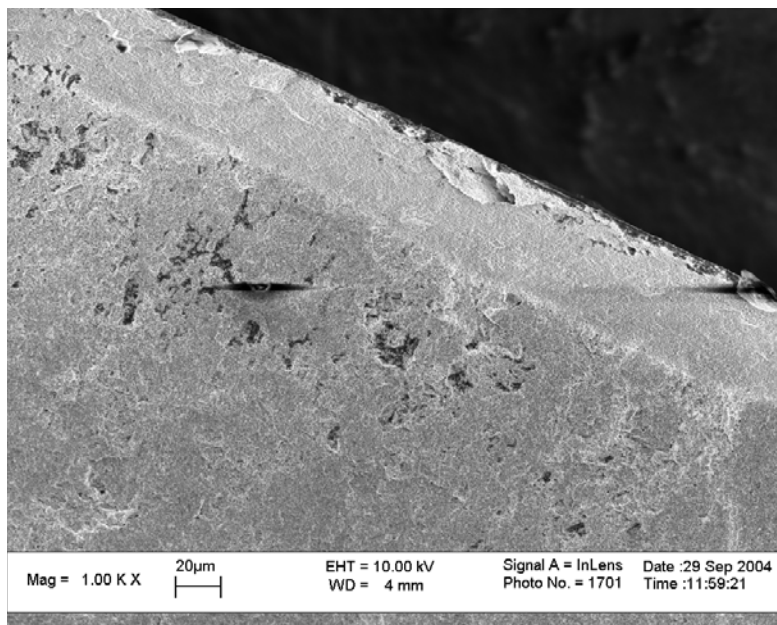


Figure 28. Micrograph of a cathode-supported thin-film cell, 20 μm BYZ supported on $\text{BaZr}_{0.40}\text{Pr}_{0.40}\text{Gd}_{0.20}\text{O}_3$.

Screening potential anode electrocatalysts (metals) for reactivity with $\text{BaZr}_{1-x}\text{Y}_x\text{O}_{3-\delta}$, fabrication compatibility, and chemical stability in fuel cell environment.

Because Ni has been established as a good catalyst for anode reaction in YSZ, it was our initial intention to use a NiO-BYZ porous support for a thin BYZ electrolyte membrane. However, according to our preliminary experiment, it was realized that NiO easily diffuses into the BYZ layer during sintering. Attempts were made to prevent this diffusion by lowering sintering temperature, however to obtain a high density layer sintering at 1600°C is needed. Therefore, we concluded that it is very difficult to use NiO as support material. Then, we tried to find alternative support material that has catalytic ability for electrode reaction. In this study, FeOx, Ni, Fe and

NiAl were examined, but all had fatal problem. Thus, we developed bi-layer and tri-layer BYZ systems with varying porosity. The support is a porous BYZ layer while the electrolyte is a fully densified layer. Figure 29 shows SEM micrographs of such systems. Future plans include impregnation techniques to incorporate a metal catalyst into the porous layer.

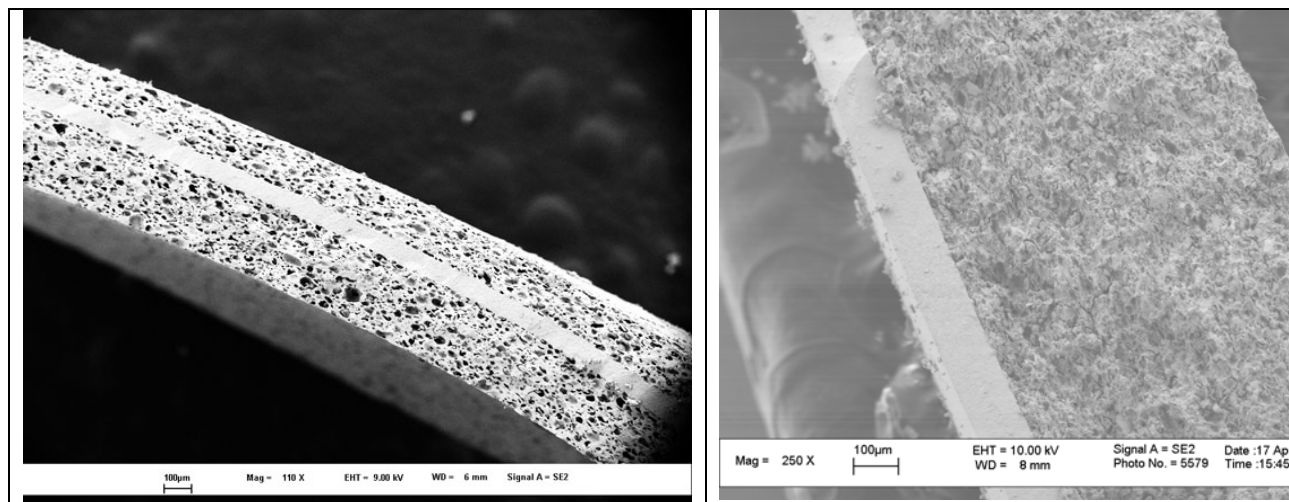


Figure 29. Cross section of 80 μm electrolyte BYZ membrane sandwiched by porous BYZ layers (a) and Cross-section of 100 μm electrolyte BYZ membrane on BYZ porous support (b).

CONCLUSIONS

A series of QM cluster, slab and periodic calculations have been carried out on relevant metals (Ba, Zr, Y, Pt, Ni), metal alloys (Y/Zr, Y/Ba, Zr/Ba, Pt/Ni, Pt/Zr), metal oxides (ZrO_2 , Y_2O_3 , BaO, NiO), pure and Y-doped BaZrO_3 . The obtained QM data were then incorporated into the ReaxFF training set.

QM calculations on BYZ periodic structures have been performed and energy barriers for the hydrogen diffusion have been calculated. The activation energy for the intra- ZrO_6 -octahedron proton transfer is found to be equal to 0.55 eV, while that for the inter- ZrO_6 -octahedra proton transfer is 0.44 eV, which is in very good agreement with the experimental value, 0.44 eV.

ReaxFF potentials have been developed for further atomistic MD simulations to study the proton transport, the role of grain boundaries and defects, structural features of grains and grain boundaries, etc. in the BYZ electrolyte and chemical reactions at the electrode/electrolyte interface.

From our ReaxFF MD simulations of the hydrogen diffusion in BYZ we found that the ReaxFF properly describes transport properties of the BYZ electrolyte and the simulated diffusion coefficients and activation energy are in good agreement with the experimental values. Our preliminary result also shows that when the hydrogen reaches the grain boundaries, it is stuck there for a relatively long time within a limited volume.

$\text{BaZr}_{1-x}\text{Y}_x\text{O}_{3-\delta}$ with $x = 0.2, 0.3, 0.4, 0.5$ have been synthesized using a modified Pechini method. We found that a single perovskite phase is formed in $\text{BaZr}_{1-x}\text{Y}_x\text{O}_{3-\delta}$.

To accelerate the densification process of BaZrO₃ ceramics at lower temperature, an initial screening of all transition elements in the series Sc to Zn has been performed. It turned out that NiO, CuO and ZnO are the most effective additives for enhancing barium zirconate densification. The enhanced densification for modified BYZ has been improved to 95% with refined mixing techniques. Densification was also achieved without the use of sintering aids, by (i) mechanical grinding of the starting powder to <50 nm (ii) use of a binder solution, (iii) pre-calcination, and (iv) avoidance of Ba loss during sintering. The optimized procedures lead to highly reproducible density and conductivity of BYZ.

A robust method for fabricating crack-free thin membranes, as well as methods for sealing anode and cathode chambers, have successfully been developed.

Several potential cathode materials for the Y-doped BaZrO₃ system have been synthesized and characterized. Of the five potential cathode materials examined BaZr_{0.55}Y_{0.15}Pr_{0.30}O₃, and BaZr_{0.70}Y_{0.15}Pr_{0.15}O₃ appear to be the most promising for further applications in proton ceramic fuel cells.

Two cathode deposition techniques based on colloidal methods were pursued for the fabrication of electrolyte-supported fuel cells. The method, in which the colloidal solution was deposited by spraying, provides better contact between the cathode and the BYZ electrolyte, especially for Y and Zr containing cathodes.

Potential anode electrocatalysts (metals) have been screened for reactivity with BaZr_{1-x}Y_xO_{3-δ}, fabrication compatibility, and chemical stability in fuel cell environment. It was found that NiO easily diffuse into the BYZ layer during sintering. Bi-layer and tri-layer BYZ systems with varying porosity have been developed.

Fuel cell test of BYZ thin film using platinum ink for both electrodes have been performed. Successful fuel cell measurements were carried out with a peak power density of 28 mW/cm². It was shown the anode rather than the cathode is the most resistive electrode.

REFERENCES

1. H. Iwahara, H. Uchida, S. Tanaka, Solid State Ionics **9-10**, 1021 (1983).
2. H. Iwahara, H. Uchida, K. Ono, K. Ogaki, J. Electrochem. Soc. **135**, 529 (1988).
3. K.-D. Kreuer, S. Adams, W. Munch, A. Fuchs, U. Klock, J. Maier, Solid State Ionics **145**, 295 (2001).
4. H.G. Bohn, T. Schober, J. Am. Ceram. Soc. **83**, 768 (2000).
5. S.M. Haile, G. Staneff, K.H. Ryu, J. Mat. Sci **36**, 1149 (2001).
6. W.G. Coors, D.W. Readey, J. Am. Ceram. Soc., **85**, 2637 (2002).
7. D. M. Ceperley and B.J. Alder, Phys. Rev. Lett. **45**, 566 (1980).
8. J.P. Perdew and A. Zunger, Phys. Rev. B **23**, 5048 (1981).
9. Jaguar 5.0, Schrodinger Inc., Portland, OR, 2000.
10. J.C. Slater, Quantum Theory for Molecules and Solids, in: The Self-Consistent Field for Molecules and Solids, vol.4, McGraw-Hill, New York, 1974.
11. A.D. Becke, Phys. Rev. A **38**, 3098 (1988).
12. S.H. Vosko, L. Wilk, M. Nusair, Can. J. Phys. **58**, 1200 (1980).
13. C. Lee, W. Yang, R.G. Parr, Phys. Rev. B **37**, 785 (1988).

14. P. A. Schultz, unpublished [a description of the method is in P.J. Feibelman, Phys. Rev. B **35**, 2626 (1987)].
15. H.G. Bohn and T. Schober, *J. Am. Ceram. Soc.* **83**, 768 (2000).
16. B.Gross, Ch. Beck, F. Meyer, Th.Krajewski, R. Hempelmann, H. Altgeld, Solid State Ionics **145**, 325 (2001).
17. V.Agarwal, M. Liu, *J. Mat. Sci.* **32**, 619 (1997).
18. K.H. Ryu, S.M. Haile, *Solid State Ionics*, **125**, 355 (1999).
19. P. Babilo and S. M. Haile, *J. Amer. Cer. Soc.* **88**, 2362-2368 (2005).

LIST OF ACRONYMS AND ABBREVIATIONS

BYZ – Y doped BaZrO₃

DFT – Density Functional Theory

GGA – generalized gradient approximation

MD – Molecular Dynamics

MEA – Membrane-Electrode Assembly

PCFC – Proton Ceramic Fuel Cell

QM – Quantum Mechanics

ReaxFF – First Principles-Based Reactive Force Field

SEM – Scanning Electron Microscopy

SOFC – Solid Oxide Fuel Cell

TGA – Thermo Gravimetric Analysis

XRD – X-ray Diffraction

YSZ – Yttria-stabilized zirconia